Merging fNIRS-EEG Brain Monitoring and Body Motion Capture to Distinguish Parkinsons Disease

Mohammadreza Abtahi, Seyed Bahram Borgheai, Roohollah Jafari, Nicholas Constant, Rassoul Diouf, Yalda Shahriari, Kunal Mankodiya

***Abstract*—Functional connectivity between the brain and body kinematics has largely not been investigated due to the requirement of motionlessness in neuroimaging techniques such as functional magnetic resonance imaging (fMRI). However, this connectivity is disrupted in many neurodegenerative disorders, including Parkinson's Disease (PD), a neurological progressive disorder characterized by movement symptoms including slowness of movement, stiffness, tremors at rest, and walking and standing instability. In this study, brain activity is recorded through functional near-infrared spectroscopy (fNIRS) and electroencephalography (EEG), and body kinematics were captured by a motion capture system (Mocap) based on an inertial measurement unit (IMU) for gross movements (large movements such as limb kinematics), and the WearUp glove for fine movements (small range movements such as finger kinematics). PD and neurotypical (NT) participants were recruited to perform 8 different movement tasks. The recorded data from each modality have been analyzed individually, and the processed data has been used for classification between the PD and NT groups. The average changes in oxygenated hemoglobin (HbO2) from fNIRS, EEG power spectral density in the Theta, Alpha, and Beta bands, acceleration vector from Mocap, and normalized WearUp flex sensor data were used for classification. 12 different support vector machine (SVM) classifiers have been used on different datasets such as only fNIRS data, only EEG data, hybrid fNIRS/EEG data, and all the fused data for two classification scenarios: classifying PD and NT based on individual activities, and all activity data fused together. The PD and NT group could be distinguished with more than 83% accuracy for each individual activity. For all the fused data, the PD and NT groups are classified with 81.23%, 92.79%, 92.27%, and 93.40% accuracy for the fNIRS only, EEG only, hybrid fNIRS/EEG, and all fused data, respectively. The results indicate that the overall performance of classification in distinguishing PD and NT groups improves when using both brain and body data.**

***Index Terms*—Brain Body fusion, Sensor fusion, fNIRS, EEG, Motion Capture.**

I. Introduction

People suffering from movement disorders have benefited from studies on neuroimaging and body motion capture techniques individually [1]–[9]. While studies using a single modality support understanding of neurological activities and movement issues, functional connectivity between the two is not yet understood. Some studies have investigated the coupling between the brain and the body with a focus on a few motor tasks of muscle contractions or small movements such as finger flexion/extension. These combined studies [10]–[17] utilized mostly electroencephalography (EEG) or magnetoencephalography (MEG) as the brain monitoring modality. However, the high sensitivity of these systems to movement artifacts prevents their robust use in experiments involving larger ranges of movement. In order to overcome this limitation in this study, functional near-infrared spectroscopy (fNIRS), and EEG have been integrated as synchronized brain monitoring systems for larger range motor tasks. The fNIRS system captures hemodynamic responses in the brain and has been shown to be less prone to motion artifacts, though low temporal resolution and delays in hemodynamic responses are well-known drawbacks of fNIRS. EEG, which provides a higher temporal resolution (256 Hz compared to 10 Hz of fNIRS) and faster electrical activity responses is synchronized with fNIRS in this study to compensate for drawbacks of fNIRS. Body kinematics are generally divided into two categories of gross motor movements and fine motor movements. Gross movements of both upper and lower limbs are recorded through a non-optical motion capture system (Mocap). The Mocap system captures gross or large range movements such as limb movements like hand pronation/supination, arm movements, and foot stomping. This system is not able to measure fine motor movements such as finger tapping, one of the most common tests in PD screening. The WearUp glove, which is integrated with flexible sensors, is therefore used to measure fine motor finger movements. This study thus records both fine and gross motor tasks, respectively using the WearUp and Mocap systems. Figure 1 shows an overview of this research fusion system.

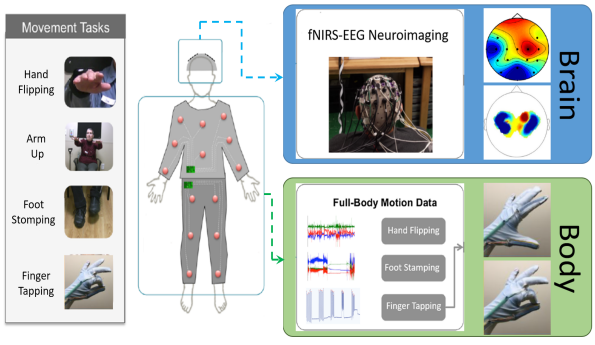

Fig. 1: Overview of the fusion system.

II. Background

Parkinson's Disease (PD) is the second most common neurodegenerative motor disorder, affecting 4 million [18]

The authors are with the department of Electrical, Computer, and Biomedical Engineering, University of Rhode Island, Kingston, RI, 02881 USA e-mail: mabtahi2012@uri.edu, kunalm@uri.edu

people worldwide. Studies suggest that approximately 0.6% of the total United States population and 0.8% of the European and Canadian population will be affected by PD by 2050 [19]. PD patients have various movement-related symptoms including resting tremor, muscle stiffness or rigidity, slowness of movement, and gait and balance problems such as shuffling, freezing or falling due to alterations in their brain-body coupling. Neuromuscular pathways responsible for transferring motor commands from and to the brain are affected in PD, which results in alterations in the coupling between the brain and the body known as cortico-muscular coherence (CMC) [20]. Coherence is the degree of time-locked correlation between two signals as a function of frequency [21]. CMC usually refers to coherence between cortical activity and muscle contractions measured by electromyogram (EMG). The coherence between cortical activity and body kinematics, cortico-kinematic coherence (CKC), uses movement sensors such as accelerometers as the kinematic measurement unit. Some abnormal CMC patterns have been reported in movement disorders such as PD [22], [23]. Most studies of CMC have utilized EEG or MEG as the brain monitoring technique and EMG to record muscle contractions [11], [13]–[15], [24], [25].

Recently, Sridharan et al. [10] measured the CMC between the MEG and EMG from six PD patients undergoing deep brain stimulation (DBS) ON and six medicated PD patients (levodopa) along with ten age-matched healthy controls. The experimental task was hand gripping. Sridharan et al. [10] calculated CMC in the beta range (13-30 Hz). Medication increased CMC values above control levels, but DBS results in lower CMC values.

The effects of subthalamic nucleus (STN) DBS on the CMC from PD patients is examined in a study from Airaksinen et al. [26]. The authors used MEG and EMG simultaneously while DBS was on and off and showed CMC peaks in the frequency range of 13-25 Hz in 15 out of the 19 patients, with a variable effect of DBS on CMC. Stronger CMC did not necessarily indicate better functionality; however, tremor and rigidity may have affected the results. The study concluded that DBS would modify CMC in advanced PD patients, but with large inter-individual variability.

Caviness et al. [21] observed an abnormal increase in the CMC of PD patients with small amplitude cortical myoclonus. The study involved PD patients with and without myoclonus and controls. Coherence peaks were observed in the 12-30 Hz band in PD patients with myoclonus, significantly greater than those in PD patients without myoclonus and controls. Caviness et al. [21] findings provide evidence that there are abnormal rhythmic activities in cortical motor areas in PD patients with myoclonus.

Marty et al. [12] measured CKC between MEG and a 3-axis accelerometer, while eleven healthy adults executed or observed a goal-directed hand action performed by an actor in front of them. Statistically significant coherence at the movement frequency and its first harmonic was observed in both conditions. This significant coherence is reported in the visual cortices, right posterior superior temporal gyrus, bilateral superior parietal lobule, and primary sensorimotor cortex.

Bourguignon et al. [16] presented CKC as a promising method for reliable and convenient functional mapping of the human motor cortex. Coherence between MEG and a 3-axis accelerometer on the right index finger showed peaks around 3-5 Hz and 6-10 Hz, corresponding to the self-paced flexion/extension of the finger at 3 Hz. Coherence was significant for all ten subjects in the contralateral hand area of the primary motor cortex.

In another study by Bourguignon et al. [27], CKC between MEG and a 3-axis accelerometer on the right index finger during fast repetitive voluntary hand movements was measured for ten healthy right-handed adults performing flexion/extension movements with their right-hand finger with and without thumb-finger touching. It was reported that the coherence values were significantly higher in the touch condition compared to the no touch condition, with the main sources of coherent activity in the left primary motor and sensory hand areas.

Another report by Bourguignon et al. [28] investigated CKC between MEG recorded from a participant viewing experimenter motion and the 3-axis accelerometer on the index finger of the experimenter. A significant peak in the coherence spectra at the flexion/extension frequency of 3 Hz and its first harmonic is strongly observable in the visual areas, as well as in the primary motor cortices of both hemispheres and in the cerebellum. All these studies examine the coupling between the brain and the body and how the correlation and coherence between brain activity and body motion are changed in PD and healthy groups. These studies do not differentiate between the two groups. This study focuses on developing a multi-modal brain-body fusion system and distinguishing PD participants from healthy participants.

III. Experiment Design

This section describes experiments on PD patients and neurotypical (NT) participants to measure brain activity and body movement. The fNIRS system used in this study is the NIRScout system (NIRx Inc., New York, NY, USA) [29]. This system utilizes 8 light sources and 8 light detectors. fNIRS system uses NIR light at two wavelengths of 760 and 850 nm and the sampling rate of 7.81 Hz. The EEG system used in this study is the g.USBAMP from g.tec [30] recording brain activity with the sampling rate of 256 Hz. WearUp is an active smart glove developed to record and detect patients hand movements such as finger tapping [31]. WearUP consists of two flexible sensors woven into a base fabric, an embedded processor with Bluetooth low energy for wireless communication of sensor data, and a power management module. In this study, a non-optical motion capture system called YEI 3-Space Mocap (YEI Technology, Portsmouth, OH, USA) [32] is used. This system consists of 17 IMU sensors that are able to record the movements of different joints of the body.

fNIRS and Mocap data have been recorded through an application protocol interface (API) that we have developed specifically, for this purpose. The API is named brain body monitoring API (BBM API). The Mocap and fNIRS systems respectively have Mocap Studio and NIRStar as native soft-

ware. However, to provide more control over the synchronization of data collection from both systems, the BBM API was developed. Two Python wrappers have been used to create the API. The Mocap sensors wrapper, named Threespace, can be found on GitHub [33]. This Python wrapper is open source and compatible with YEI 3-space Mocap sensors. The fNIRS wrapper comes as a software add-on to the NIRStar that allows data to be streamed through an API called the Lab Streaming Layer (LSL). The LSL API is also available on Github [34]. Figure 2 shows an overview of the BBM API. EEG data has simultaneously been recorded through the system from g.tec Inc. and the synchrony of the EEG and the API is provided through a trigger output from the amplifier of the EEG system. 11 PD patients without deep brain stimulation (DBS) and 10 NT participants were recruited. PD recruitment criteria were a diagnosis of PD and the lack of DBS implants. The criteria for NT group recruitment was having no known neurological disorders. All participants consented prior to the experiment according to the institutional review board (IRB) requirements and approval at the University of Rhode Island.

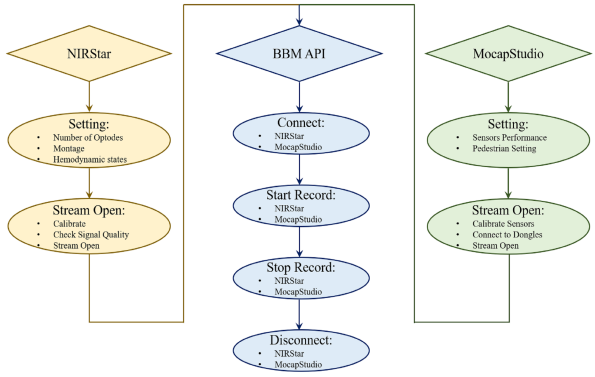

Fig. 2: Overview of the BBM application protocol interface.

Due to technical problems and some data loss, data from subjects NT10, PD10, and PD11 have been excluded. Therefore, the remaining of this article is based on the data from 9 PD and 9 NT participants. Table I shows the information about the participants. The protocol of the experiment consists of 8 different motor tasks related to the Unified Parkinson's Disease Rating Scale (UPDRS) motor examination. The tasks are as follows and the experiment is conducted by performing the tasks in the order mentioned here (please note the activity indexes as they will be referred to in the results section):

- A1. Right hand finger tapping
- A2. Left hand finger tapping
- A3. Right hand flipping
- A4. Right arm movement
- A5. Left hand flipping
- A6. Left arm movement
- A7. Right foot stomping
- A8. Left foot stomping

Finger tapping kinematics were recorded by the WearUp glove developed through this research and the other movements were recorded by the Mocap system. fNIRS and EEG neuroimaging optodes are placed over the motor cortex based on the International 10-20 system to capture movement-related neural activity. The placement of fNIRS optodes produces 18 channels of data.

TABLE I: Participant demographics.

Group PD	Gender	Age	Year of Diagnosis		Group NT	Gender	Age
PD1	F	72	2002		NT1	M	71
PD2	F	78	2017		NT2	M	70
PD3	F	73	2017		NT3	F	62
PD4	M	67	2013		NT4	F	81
PD5	F	76	2015		NT5	M	65
PD6	M	56	2015		NT6	F	62
PD7	M	80	2008		NT7	F	66
PD8	F	76	2005		NT8	F	56
PD9	F	79	2008		NT9	F	56
PD10	M	87	2017		NT10	F	72
PD11	M	76	2018				

Unfortunately, one of the light sources (S7 as indicated in Figure 3) experienced malfunction in the middle of the study. Therefore, two channels of fNIRS data created by S7 (channels of S7-D5, and S7-D7) were excluded from processing. 13 EEG electrodes have been used in the locations of FC3, FC4, C1, Cz, C2, C3, C4, CP1, CP2, CP3, CP4, P3, and P4. The placement of fNIRS optodes and EEG electrodes is shown in Figure 3.

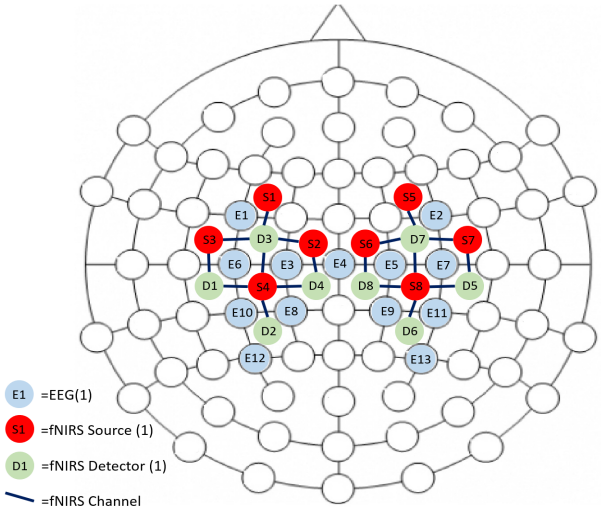

Fig. 3: The montage of fNIRS and EEG electrodes.

The participants were instructed about how to perform each task prior to the experiment. Participants were given time to practice and become familiar with the tasks, but no data was collected during the practice time. 20 seconds no movement recording time has been used as the baseline before the protocol of the experiment starts. Participants were asked to follow the visual cues on the screen to perform each task for 5 trials, each consisting of 10 seconds activity followed by 10 seconds rest. The participants were instructed to perform each task at their own comfortable pace. A green circle on the screen indicates participants should perform the task, and a blank white screen commands to stop and rest. Figure 4 shows the protocol of the experiment.

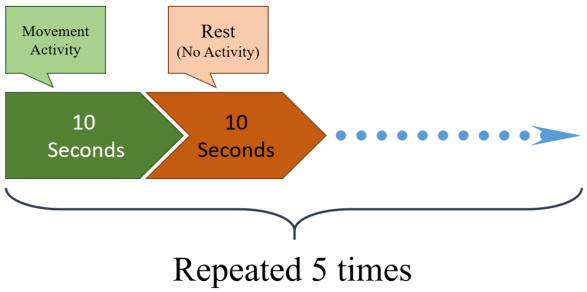

Fig. 4: Timings of the experiment protocol.

IV. Methods

This section explains the process of preparing the data from each modality for classification between the PD and NT groups.

A. fNIRS Analysis

fNIRS system utilizes NIR light at two wavelengths of 760 and 850 nm. The oxygenated hemoglobin (HbO2) and deoxygenated hemoglobin (Hb) can be calculated based on the Beer-Lambert law. Preprocessing includes removing environment noise and physiological noises such as heartbeat, Mayor wave, and respiration rate. A 4th order band-pass Butterworth filter is first applied to the data with cutoff frequencies of 0.1-0.4 Hz to remove these sources of noise [35], [36]. The extinction coefficient of hemoglobin needs to be defined in order to use the modified Beer-Lambert law to calculate HbO2 and Hb concentrations. There are some small differences in the extinction coefficients of hemoglobin reported in the literature [37]–[43]. The reported values in [39] have been used in order to calculate the HbO2 and Hb concentrations as suggested by NIRx. Yet another parameter setting is DPF, which takes into account the additional average distance light travels due to scattering beyond the linear distance between a source and receiver. Values representative of reports described in the literature [44]–[46] have been chosen as follows:

- DPF for WL1: 7.25
- DPF for WL2: 6.37

It deserves noting that the true value will depend on head shape, skull thickness, and properties of underlying tissues which are beyond the scope of this study. After setting all the parameters, the HbO2 and Hb concentrations were calculated.

B. EEG Analysis

EEG is collected using the BCI2000 software [47] at a sampling rate of Fs= 256 Hz. The data analysis starts with detrending the data, done on the normalized signal using the z-score. The z-score is calculated as $z = (X - \mu)/\sigma$, where z is the z-score, X is the value of the element, μ is the population mean, and σ is the standard deviation. After detrending the signal, a Finite Impulse Response (FIR) band-pass filter with order 3 and cutoff frequencies of 1 and 99 Hz have been applied to the data. Next, the power spectral density (PSD) of the signal is calculated. PSD provides information regarding the distribution of average power as a function of frequency. It can be calculated as the Fourier transform of the autocorrelation function. After calculating the PSD for the EEG signal, the power in the frequency bands of Theta (4-7 Hz), Alpha (8-15 Hz), and Beta (16-30 Hz) [48] are calculated. The power in these bands is used to classify the two groups of participants.

C. Mocap Analysis

Mocap data has been recorded from 3 sensors with the actual sampling rate of 50 Hz. The data is upsampled to 256 Hz to match the frequency of EEG recording. The locations of the sensors are as follow based on the activity.

- Sensor 1: Around hand, or around foot
- Sensor 2: Lower arm (below elbow), or lower leg (below the knee)
- Sensor 3: Upper arm, or upper leg

Each sensor provides three degrees of freedom for each of acceleration, gyroscope, and magnetometer. The data has been normalized and detrended and the acceleration vector has been calculated to be used for classification.

D. WearUp Analysis

Flex data was collected from the glove at a variable sampling rate of approximately 50 Hz. A resampling method to match the 256 Hz sampling frequency of EEG has been used. Standard preprocessing steps such as z-score normalization and detrending were also performed on the data.

E. Classification

Support Vector Machine (SVM) is used as the classification method to distinguish the PD and NT groups based on the fused data. The general concept of the SVM is that the system uses a training dataset which is labeled with different categories. This training set may be part of the original dataset. Then, after the system is trained, it will be tested on the rest of the original dataset to predict the data labels. In this study, several learning algorithms have been implemented as the grid search in the support vector machines in order to find which learning algorithm has better performance. By applying the Lagrangian optimization theory to a linear support vector machine and using the kernel functions, it is possible to classify datasets which are not linearly separable. Table II shows the learning algorithms used in this study with their complexity index, which we will refer to in the results section.

The main goal of this study was to distinguish the PD and NT groups using our brain-body fused data. To achieve this goal, the data from all the devices have been fused together for classification. As this dataset is big data and the classification of this big data needs exceptional computing, the data size was reduced by averaging all data in one-second intervals. That is, all the data points in a one-second window are averaged and treated as single data points. This averaging results in an HbO2 concentration for each of 16 fNIRS channels (16 features), Theta, Alpha, and Beta frequency band EEG power on each of 13 EEG channels (13x3 = 39 features), and the activity-based

TABLE II: Different methods of classification used in this study.

Index	Kernel Name	Kernel Function	Degree	Cost Constant
1	Linear Kernel	$k(\vec{x},\vec{y}) = \vec{x}\cdot\vec{y}$	–	1
2	Linear Kernel	$k(\vec{x},\vec{y}) = \vec{x}\cdot\vec{y}$	–	10
3	Linear Kernel	$k(\vec{x},\vec{y}) = \vec{x}\cdot\vec{y}$	–	100
4	Polynomial Kernel	$k(\vec{x},\vec{y}) = (\vec{x}\cdot\vec{y}+c)^d$	2	1
5	Polynomial Kernel	$k(\vec{x},\vec{y}) = (\vec{x}\cdot\vec{y}+c)^d$	2	10
6	Polynomial Kernel	$k(\vec{x},\vec{y}) = (\vec{x}\cdot\vec{y}+c)^d$	2	100
7	Polynomial kernel	$k(\vec{x},\vec{y}) = (\vec{x}\cdot\vec{y}+c)^d$	3	1
8	Polynomial Kernel	$k(\vec{x},\vec{y}) = (\vec{x}\cdot\vec{y}+c)^d$	3	10
9	Polynomial kernel	$k(\vec{x},\vec{y}) = (\vec{x}\cdot\vec{y}+c)^d$	3	100
10	Radial kernel	$k(\vec{x},\vec{y}) = e^{-(\vec{x}-\vec{y})^2/2\sigma^2)}$	–	1
11	Radial kernel	$k(\vec{x},\vec{y}) = e^{-(\vec{x}-\vec{y})^2/2\sigma^2)}$	–	10
12	Radial Kernel	$k(\vec{x},\vec{y}) = e^{-(\vec{x}-\vec{y})^2/2\sigma^2)}$	–	100

Mocap acceleration or glove flex data (1 feature). Fusing all the data provides a dataset with 16 + 39 + 1 = 56 features. Participants were asked to perform each of the 8 activities for 5 trials. The first 3 trials of each activity create the training dataset for the classifier, and the last 2 trials are left for testing the performance of the classifier. The classification between PD and NT group was performed in two different scenarios: 1. Classifying the two groups in each individual activity. This means that the data from all of the modalities recorded from all of the participants related to a specific task has been merged together in order to create the training and testing datasets, and all of the classifiers mentioned in Table II have been applied on them. 2. Classifying the two groups for all the activities combined. This means that all the data from all the participants for all the activities have been merged together to create the training and testing datasets. The classifiers in Table II have again been applied to this data.

V. Results and Discussion

All the data are analyzed based on the methods described in the previous section and are fused together for classification in order to distinguish between the PD and NT groups. Figure 5 shows the performance of the BBM API by plotting the time series data of the Mocap and fNIRS before and after the interpolation and upsampling. It can be seen that the data is synchronized well without any changes on the time series.

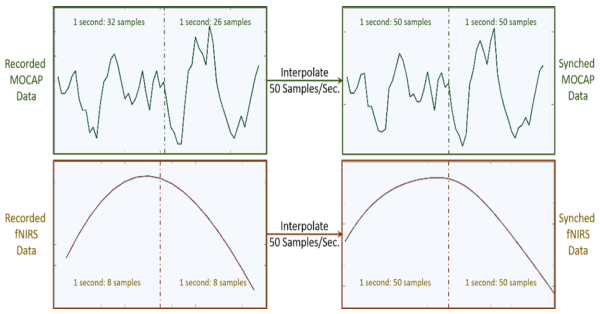

Fig. 5: Performance of BBM API by showing the synchronization method. 2 seconds of the MOCAP and fNIRS are shown. Each 1 second window of the data is interpolated to 50 samples separately.

Figure 6 shows the synchronized fNIRS hemodynamic response and the Mocap data for a cycle of 20 seconds no movement (used as the baseline) followed by 10 seconds of right foot stomping. It is clear from the time series data that the hemodynamic response is in synchrony with the body movement. Please note the delay in hemodynamic response for getting to the peak after initiation of the movement.

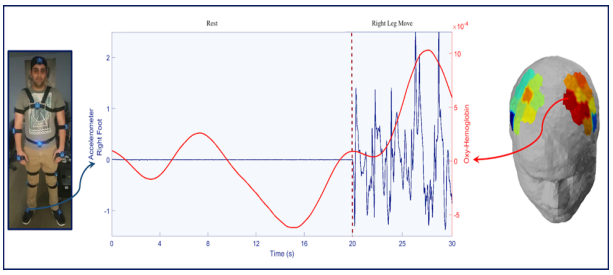

Fig. 6: Accelerometer (Blue), and OxyHemoglobin (Red) data for 20 seconds no movement followed by 10 seconds right leg activity (foot stomping).

Figure 7 shows another time series data for a cycle of rest period followed by finger tapping for a participant of the NT group (top panel) and PD group (bottom panel).

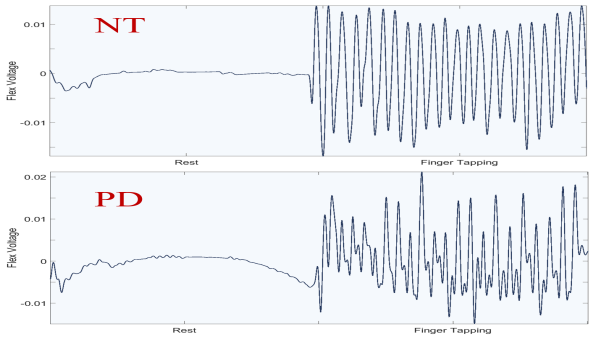

Fig. 7: Flex sensor data of the smart glove for a cycle of rest followed by finger tapping. Top panel shows the data from NT group, bottom panel shows data from PD group.

12 different SVM classifiers have been used in this study, and they are introduced in Table II. Classifiers will be referred to by index. The classification has been performed in two different scenarios. One is to distinguish PD and NT group based on each of the 8 activities separately, and the second is to distinguish PD and NT group based on all the data together.

A. Activity Based Classification

Table III reports the accuracy, sensitivity, and specificity of the 12 classifiers to distinguish PD and NT group based on the data from all of the modalities for each activity separately.

It can be seen that for each activity, the PD and NT group can be distinguished with at least 83% accuracy. It is also noteworthy to observe that by using a more complex classifier (higher index), the sensitivity and specificity percentages get closer, indicating an equal number of false positive (FP) and false negative (FN) predictions. This reveals the optimal performance of the classifier.

TABLE III: Accuracy of all the 12 classifiers on the data from all of the modalities for each activity.

SVM Index	A1	A2	A3	A4	A5	A6	A7	A8
1	76.80%	80.69%	79.86%	83.33%	82.08%	81.94%	77.36%	78.75%
2	76.80%	81.25%	79.72%	82.91%	82.22%	81.80%	77.50%	79.58%
3	76.66%	81.25%	79.86%	83.05%	81.66%	82.08%	76.94%	79.30%
4	83.19%	84.02%	80.27%	83.61%	85.69%	84.58%	81.66%	86.52%
5	86.94%	87.77%	87.50%	85.27%	88.61%	88.33%	85.13%	89.72%
6	85.69%	88.75%	87.77%	85%	88.61%	86.11%	85.27%	90.83%
7	79.44%	82.36%	78.61%	78.19%	76.80%	79.02%	79.30%	83.19%
8	74.72%	83.33%	84.58%	82.63%	82.50%	82.08%	80.55%	86.52%
9	73.75%	83.47%	80.97%	80.55%	81.94%	80.83%	77.91%	87.77%
10	85.13%	89.58%	87.22%	90.27%	88.19%	88.75%	88.47%	90.27%
11	85.55%	91.25%	88.75%	91.38%	90.83%	90.13%	90%	92.63%
12	83.61%	90.55%	87.77%	91.66%	90%	91.11%	88.61%	92.50%

B. All Data Classification

In this section, the data from all the 8 activities are merged to determine if the PD and NT groups could be distinguished based on the combined activity data. The classification has been applied to four different datasets: 1. Dataset including all the activities for only fNIRS. 2. Dataset including all the activities for only EEG. 3. Dataset including all the activities for hybrid fNIRS/EEG. 4. Dataset including all the activities for all fused data (fNIRS/EEG/kinematics). Figure 8(A) shows the performance of all the 12 classifiers on the dataset containing only fNIRS data. It is clear that by using the most complex classifier (radial kernel), the accuracy, sensitivity, and specificity performance measures converge, indicating optimal performance. The highest accuracy in distinguishing between the PD and NT groups using only fNIRS data is 81.23% with 83.57% and 78.89% sensitivity and specificity, respectively, using the SVM with index 12.

Figure 8(B) shows the performance of all the 12 classifiers on the dataset containing only EEG data. The highest accuracy in distinguishing between the PD and NT groups using only EEG data is 92.79% with 93.12 and 92.46 sensitivity and specificity, respectively.

Figure 8(C) shows the performance of all 12 classifiers on the dataset containing hybrid of fNIRS and EEG data. The highest accuracy in distinguishing between the PD and NT groups using hybrid of fNIRS and EEG data is 92.27% with 91.35 % and 93.19% sensitivity and specificity, respectively.

Figure 8(D) shows the performance of all 12 classifiers on the dataset containing all the recorded data. The highest accuracy in distinguishing between the PD and NT groups using all the data is 93.40% with 93.78% and 93.02% sensitivity and specificity, respectively.

It can be observed that classifying data with all the modalities improves the accuracy of classification between the PD and NT groups. This reveals the importance and critical role of each modality used in this study.

VI. Conclusion

The objective of this study was to perform an experiment on PD patients and NT group aiming to distinguish between PD and NT based on the fused brain and body data. The brain imaging systems used for this experiment were fNIRS and EEG. Body kinematics were measured with a Mocap system and the WearUp glove. 11 PD patients and 10 NT participants were recruited to perform 8 motor tasks on upper and lower limbs of both sides of the body. The data were recorded through the developed API (BBM API) and synchronized using the developed algorithms. HbO2 concentration from fNIRS data and PSD in the frequency bands of Theta, Alpha, and Beta were extracted from EEG data. The acceleration vector was calculated based on the triaxial accelerometer measures of the Mocap, and the flex sensor voltage was used from the WearUp glove. The data from all these modalities have been fused and averaged over a one-second-long moving window. The final processed data were used for classification. The goal of classification was to distinguish between the PD and NT groups.

12 different SVM classifiers were trained on the first three trials of the data, and the performance of the classifier was tested on the last two trials. The classification was performed in two different scenarios of single activity based classification, and classification of the full combined data across all activities.

In single activity classification, the data from each activity were used separately to train and test the classifiers, and the results show that the PD and NT group can be distinguished with at least 83% accuracy for each activity.

Full data classification has been performed on four different scenarios: fNIRS only, EEG only, hybrid fNIRS and EEG, and all the fused data. The optimal accuracy in distinguishing the PD and NT groups is respectively 81.23%, 92.79%, 92.27%, and 93.40% for the four scenarios.

The lower accuracy of the fNIRS only classification might be due to the nature of this data. fNIRS measures changes in HbO2 levels in the blood. This is a hydraulic system with delays in hemodynamic flow. The delay of hemodynamic responses based on changes in HbO2 levels can be seen in the cross-correlation of the fNIRS data and Mocap data. Cross-correlation measures the similarity of two series as a function of the displacement of one relative to the other. Therefore, the peak time in the cross-correlation of two series is the hemodynamic signal delay.

Many studies have individually measured body kinematics in people with movement disorders [7], [8], [49]–[52] measured brain activity in movement disorders, or discriminated different activities based on brain activity [2], [3], [5], [53]–[58]. This study merges these separate studies together to provide clear insight about the synchrony between brain and body. Some studies have measured brain-body synchrony, but they usually utilize one modality of brain monitoring such as EEG or MEG, and one modality of body kinematic recording related to gross motor tasks or muscle contractions by electromyogram (EMG) [10]–[16], [24]–[28].

This study is among few studies, if not the only and the first study, to fuse brain and body data with two different modalities of brain imaging and to measure both fine and gross movements. The promising results show the feasibility of using all different recording modalities. Our future work includes a more thorough data recording from a bigger population of patients and neurotypical groups with a balance between male and female participants. More rigorous signal processing and analyzing of each individual modality data would be beneficial to extract features to be used in classification and provide better results. Different classification methods such as Linear

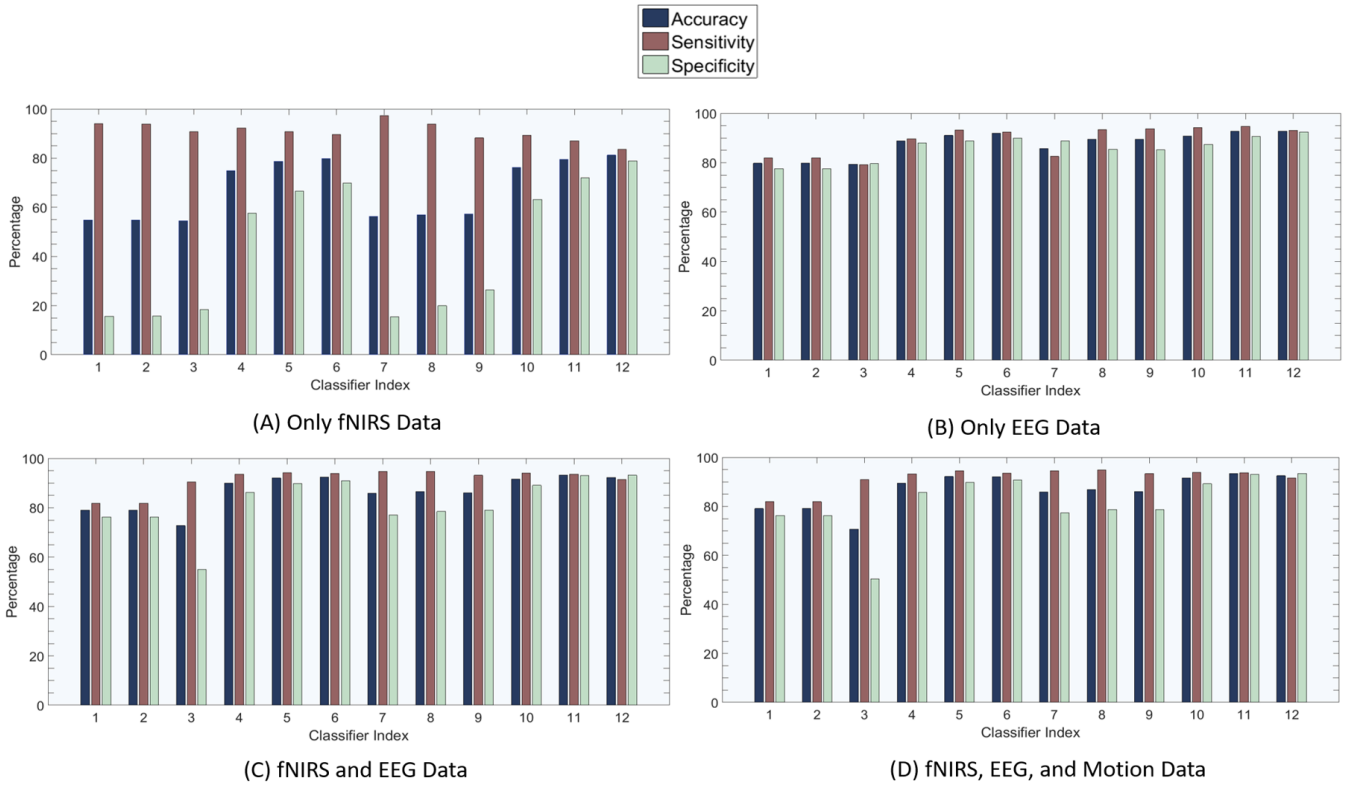

Fig. 8: Performance of all 12 classifiers on the dataset containing (A)Only fNIRS data, (B)Only EEG data, (C)Hybrid fNIRS/EEG data, and (D)All fNIRS, EEG, Motion data.

Discriminant Analysis, Neural Networks, and Deep Learning will be applied to compare the performance of the classifiers. Measuring the synchrony between brain and body as discussed in the background is another main future objective of this research.

ACKNOWLEDGMENT

This material is based upon work supported by the National Science Foundation under Grant Numbers (#1652538 and #1565962). The authors would like to thank Alyssa Zisk for proofreading the document.

REFERENCES

[1] M. A. Sommer and R. H. Wurtz, Brain circuits for the internal monitoring of movements, Annu. Rev. Neurosci., vol. 31, pp. 317338, 2008.
[2] M. R. DeLong, Primate models of movement disorders of basal ganglia origin, Trends in neurosciences, vol. 13, no. 7, pp. 281285, 1990.
[3] K. Leenders, A. Palmer, N. a. Quinn, J. Clark, G. Firnau, E. Garnett, C. Nahmias, T. Jones, and C. Marsden, Brain dopamine metabolism in patients with parkinsons disease measured with positron emission tomography. Journal of Neurology, Neurosurgery & Psychiatry, vol. 49, no. 8, pp. 853860, 1986.
[4] S. M. Rao, A. R. Mayer, and D. L. Harrington, The evolution of brain activation during temporal processing, Nature neuroscience, vol. 4, no. 3, p. 317, 2001.
[5] U. Sabatini, K. Boulanouar, N. Fabre, F. Martin, C. Carel, C. Colonnese, L. Bozzao, I. Berry, J. Montastruc, F. Chollet, et al., Cortical motor reorganization in akinetic patients with parkinsons disease: a functional mri study, Brain, vol. 123, no. 2, pp. 394403, 2000.
[6] B. J. French and K. R. Ferguson, System and method for tracking and assessing movement skills in multidimensional space, Oct. 30 2001, uS Patent 6,308,565.
[7] B. Galna, G. Barry, D. Jackson, D. Mhiripiri, P. Olivier, and L. Rochester, Accuracy of the microsoft kinect sensor for measuring movement in people with parkinsons disease, Gait & posture, vol. 39, no. 4, pp. 10621068, 2014.
[8] P. E. OSuilleabhain and R. B. Dewey Jr, Validation for tremor quantification of an electromagnetic tracking device, Movement disorders: official journal of the Movement Disorder Society, vol. 16, no. 2, pp. 265271, 2001.
[9] M. B. Del Rosario, S. J. Redmond, and N. H. Lovell, Tracking the evolution of smartphone sensing for monitoring human movement, Sensors, vol. 15, no. 8, pp. 18 90118 933, 2015.
[10] K. S. Sridharan, A. Hjlund, E. L. Johnsen, N. Sunde, S. Beniczky, and K. stergaard, Corticomuscular coherence during hand gripping with dbs and medication in pd patients, in Neuroscience day 2016, 2016.
[11] R. Kristeva, L. Patino, and W. Omlor, Beta-range cortical motor spectral power and corticomuscular coherence as a mechanism for effective corticospinal interaction during steady-state motor output, Neuroimage, vol. 36, no. 3, pp. 785792, 2007.
[12] B. Marty, M. Bourguignon, V. Jousmki, V. Wens, M. O. de Beeck, P. Van Bogaert, S. Goldman, R. Hari, and X. De Tige, Cortical kinematic processing of executed and observed goal-directed hand actions, Neuroimage, vol. 119, pp. 221228, 2015.
[13] Y. Zheng, L. Gao, G. Wang, Y. Wang, Z. Yang, X. Wang, T. Li, C. Dang, R. Zhu, and J. Wang, The influence of unilateral contraction of hand muscles on the contralateral corticomuscular coherence during bimanual motor tasks, Neuropsychologia, vol. 85, pp. 199207, 2016.
[14] Y. Xu, V. M. McClelland, Z. Cvetkovic, and K. R. Mills, Corticomuscular coherence with time lag with application to delay estimation, IEEE Transactions on Biomedical Engineering, vol. 64, no. 3, pp. 588600, 2017.
[15] T. Yoshida, K. Masani, K. Zabjek, R. Chen, and M. R. Popovic, Dynamic cortical participation during bilateral, cyclical ankle movements: effects of aging, Scientific reports, vol. 7, p. 44658, 2017.
[16] M. Bourguignon, X. De Tige, M. O. de Beeck, B. Pirotte, P. Van Bogaert, S. Goldman, R. Hari, and V. Jousmki, Functional motor-cortex mapping using corti-cokinematic coherence, Neuroimage, vol. 55, no. 4, pp. 14751479, 2011.

[17] D. Borthakur, Quantifying the effects of motor tasks on corticokinematic coherence in parkinsons disease, 2018.

[18] E. Dorsey, R. Constantinescu, J. Thompson, K. Biglan, R. Holloway, K. Kieburtz, F. Marshall, B. Ravina, G. Schifitto, A. Siderowf, et al., Projected number of people with parkinson disease in the most populous nations, 2005 through 2030, Neurology, vol. 68, no. 5, pp. 384386, 2007.

[19] J.-P. Bach, U. Ziegler, G. Deuschl, R. Dodel, and G. Doblhammer-Reiter, Projected numbers of people with movement disorders in the years 2030 and 2050, Movement Disorders, vol. 26, no. 12, pp. 22862290, 2011.

[20] A. Schnitzler and J. Gross, Normal and pathological oscillatory communication in the brain, Nature reviews neuroscience, vol. 6, no. 4, p. 285, 2005.

[21] J. N. Caviness, C. H. Adler, M. N. Sabbagh, D. J. Connor, J. L. Hernandez, and T. D. Lagerlund, Abnormal corticomuscular coherence is associated with the small amplitude cortical myoclonus in parkinsons disease, Movement Disorders, vol. 18, no. 10, pp. 11571162, 2003.

[22] P. Brown, S. Farmer, D. Halliday, J. Marsden, and J. Rosenberg, Coherent cortical and muscle discharge in cortical myoclonus, Brain, vol. 122, no. 3, pp. 461472, 1999.

[23] P. Brown, Muscle sounds in parkinsons disease, The lancet, vol. 349, no. 9051, pp. 533535, 1997.

[24] T. Yoshida, K. Masani, K. Zabjek, R. Chen, and M. R. Popovic, Dynamic increase in corticomuscular coherence during bilateral, cyclical ankle movements, Frontiers in human neuroscience, vol. 11, p. 155, 2017.

[25] M. A. Perez, D. S. Soteropoulos, and S. N. Baker, Corticomuscular coherence during bilateral isometric arm voluntary activity in healthy humans, Journal of neurophysiology, vol. 107, no. 8, pp. 21542162, 2012.

[26] K. Airaksinen, J. P. Mkel, J. Nurminen, J. Luoma, S. Taulu, A. Ahonen, and E. Pekkonen, Cortico-muscular coherence in advanced parkinsons disease with deep brain stimulation, Clinical Neurophysiology, vol. 126, no. 4, pp. 748755, 2015.

[27] M. Bourguignon, V. Jousmki, M. O. de Beeck, P. Van Bogaert, S. Goldman, and X. De Tige, Neuronal network coherent with hand kinematics during fast repetitive hand movements, Neuroimage, vol. 59, no. 2, pp. 16841691, 2012.

[28] M. Bourguignon, X. De Tige, M. O. de Beeck, P. Van Bogaert, S. Goldman, V. Jousmki, and R. Hari, Primary motor cortex and cerebellum are coupled with the kinematics of observed hand movements, Neuroimage, vol. 66, pp. 500507, 2013.

[29] Nirscout system, nirx inc.:, https://nirx.net/.

[30] "g.USBAMP system, g.tec:," https://www.gtec.at/product/g-usbamp-research/.

[31] M. Abtahi, N. Constant, J. V. Gyllinsky, B. Paesang, S. E. DAndrea, U. Akbar, and K. Mankodiya, Wearup: Wearable e-textiles for telemedicine intervention of movement disorders, in Wearable Technology in Medicine and Healthcare. Elsevier, 2018, pp. 173192.

[32] Yei 3-space mocap sensors:, https://yostlabs.com/product/3-space-mocap-starter-bundle/.

[33] Mocap sensors wrapper, threespace, https://github.com/Knio/threespace.

[34] Lab streaming layer for nirstar15, https://github.com/sccn/labstreaminglayer.

[35] N. Naseer and K.-S. Hong, fnirs-based brain-computer interfaces: a review, Frontiers in human neuroscience, vol. 9, p. 3, 2015.

[36] S. D. Power, A. Kushki, and T. Chau, Towards a system-paced near-infrared spectroscopy braincomputer interface: differentiating prefrontal activity due to mental arithmetic and mental singing from the no-control state, Journal of neural engineering, vol. 8, no. 6, p. 066004, 2011.

[37] J. Schmitt, Optical measurement of blood oxygenation by implantable telemetry, Technical Report G55815, Stanford., 1986.

[38] S. Takatani and M. D. Graham, Theoretical analysis of diffuse reflectance from a two-layer tissue model, IEEE Transactions on Biomedical Engineering, no. 12, pp. 656664, 1979.

[39] N. Kollias and W. Gratzer, Tabulated molar extinction coefficient for hemoglobin in water, Wellman Laboratories, Harvard Medical School, Boston, vol. 5, pp. 150161, 1999.

[40] M. K. Moaveni, A multiple scattering field theory applied to whole blood. 1971.

[41] M. Cope, The application of near infrared spectroscopy to non invasive monitoring of cerebral oxygenation in the newborn infant, Department of Medical Physics and Bioengineering, vol. 342, 1991.

[42] W. Zijlstra, A. Buursma, and W. Meeuwsen-Van der Roest, Absorption spectra of human fetal and adult oxyhemoglobin, de-oxyhemoglobin, carboxyhemoglobin, and methemoglobin. Clinical chemistry, vol. 37, no. 9, pp. 16331638, 1991.

[43] S. Wray, M. Cope, D. T. Delpy, J. S. Wyatt, and E. O. R. Reynolds, Characterization of the near infrared absorption spectra of cytochrome aa3 and haemoglobin for the non-invasive monitoring of cerebral oxygenation, Biochimica et Biophysica Acta (BBA)-Bioenergetics, vol. 933, no. 1, pp. 184192, 1988.

[44] M. Essenpreis, C. Elwell, M. Cope, P. Van der Zee, S. Arridge, and D. Delpy, Spectral dependence of temporal point spread functions in human tissues, Applied optics, vol. 32, no. 4, pp. 418425, 1993.

[45] M. Kohl, C. Nolte, H. R. Heekeren, S. Horst, U. Scholz, H. Obrig, and A. Villringer, Determination of the wavelength dependence of the differential pathlength factor from near-infrared pulse signals, Physics in Medicine & Biology, vol. 43, no. 6, p. 1771, 1998.

[46] H. Zhao, Y. Tanikawa, F. Gao, Y. Onodera, A. Sassaroli, K. Tanaka, and Y. Yamada, Maps of optical differential pathlength factor of human adult forehead, somatosensory motor and occipital regions at multi-wavelengths in nir, Physics in Medicine & Biology, vol. 47, no. 12, p. 2075, 2002.

[47] G. Schalk, D. J. McFarland, T. Hinterberger, N. Birbaumer, and J. R. Wolpaw, Bci2000: a general-purpose brain-computer interface (bci) system, IEEE Transactions on biomedical engineering, vol. 51, no. 6, pp. 10341043, 2004.

[48] G. Deuschl, "Recommendations for the practice of clinical neurophysiology," Guidelines of the International Federation of Clinical Neurophysiology, 1999.

[49] J. Hermsdrfer, N. Mai, J. Spatt, C. Marquardt, R. Veltkamp, and G. Goldenberg, Kinematic analysis of movement imitation in apraxia, Brain, vol. 119, no. 5, pp. 15751586, 1996.

[50] R. Agostino, A. Curr, M. Giovannelli, N. Modugno, M. Manfredi, and A. Berardelli, Impairment of individual finger movements in parkinsons disease, Movement disorders, vol. 18, no. 5, pp. 560565, 2003.

[51] L. Rnnqvist and B. Rsblad, Kinematic analysis of unimanual reaching and grasping movements in children with hemiplegic cerebral palsy, Clinical Biomechanics, vol. 22, no. 2, pp. 165175, 2007.

[52] N. J. Rinehart, M. A. Bellgrove, B. J. Tonge, A. V. Brereton, D. Howells-Rankin, and J. L. Bradshaw, An examination of movement kinematics in young people with high-functioning autism and aspergers disorder: further evidence for a motor planning deficit, Journal of autism and developmental disorders, vol. 36, no. 6, pp. 757767, 2006.

[53] V. Kaiser, G. Bauernfeind, A. Kreilinger, T. Kaufmann, A. Kbler, C. Neuper, and G. R. Mller-Putz, Cortical effects of user training in a motor imagery based braincomputer interface measured by fnirs and eeg, Neuroimage, vol. 85, pp. 432444, 2014.

[54] M. Abtahi, A. Amiri, D. Byrd, and K. Mankodiya, "Hand Motion Detection in fNIRS Neuroimaging Data," Healthcare, vol. 5, no. 2, p. 20. Multidisciplinary Digital Publishing Institute, 2017.

[55] K.-S. Hong, N. Naseer, and Y.-H. Kim, Classification of prefrontal and motor cortex signals for three-class fnirsbci, Neuroscience letters, vol. 587, pp. 8792, 2015.

[56] J. A. Pineda, B. Allison, and A. Vankov, The effects of self-movement, observation, and imagination on/spl mu/rhythms and readiness potentials (rps): toward a brain-computer interface (bci), IEEE Transactions on Rehabilitation Engineering, vol. 8, no. 2, pp. 219222, 2000.

[57] C. Guger, W. Harkam, C. Hertnaes, and G. Pfurtscheller, Prosthetic control by an eeg-based brain-computer interface (bci), in Proc. aaate 5th european conference for the advancement of assistive technology. Citeseer, 1999, pp. 36.

[58] M. J. Khan, M. J. Hong, and K.-S. Hong, Decoding of four movement directions using hybrid NIRS-EEG brain-computer interface, Frontiers in Human Neuroscience, vol. 244, article no. 8, 2014.

Mohammadreza Abtahi received his B.Sc. in Electrical Engineering from Sharif University of Technology, Iran, in 2012, M.Sc. and Ph.D. in Electrical Engineering from the University of Rhode Island, RI, USA, in 2014 and 2018, respectively. He has received a certificate in Neuroscience from the Interdisciplinary Neuroscience Program, University of Rhode Island in 2018.

He is currently serving as a Research and Development Scientist in medical device industry. His research interests include brain imaging, neural engineering, Brain-Computer Interface, biosignal processing, machine learning, wearable sensors, and medical device development.

Seyed Bahram Borgheai received his B.Sc. in Electrical Engineering from Sharif University of Technology, Iran, in 1999, M.Sc. in Biomedical Engineering from Tehran University, Iran, in 2002, M.Sc. and Ph.D. in Philosophy of Science from Sharif University of Technology, Iran, in 2008 and 2017, respectively.
He is currently working toward the second Ph.D. with the Department of Electrical, Computer, and Biomedical Engineering, University of Rhode Island, RI, USA. His main research interests are evaluating cognitive markers to facilitate applications of BCI systems.

Roohollah Jafari received his B.Sc. degree in Electrical and Communication Engineering from the Isfahan University of Technology, Iran, in 2012, and M.Sc. degree in Bioelectrics from Tehran University, Iran, in 2015. He is currently working toward the Ph.D. degree with the Department of Electrical, Computer, and Biomedical Engineering, University of Rhode Island, RI, USA. His research interests include Biomedical Signal Processing, Biological Systems Modeling, Computational Neuroscience, Brain Computer Interface (BCI) and Brain Mapping.

Nicholas Constant (S13) received his B.Sc. (2015) and M.Sc. (2017) in Electrical Engineering from the University of Rhode Island. He is currently working toward the Ph.D. degree with the Department of Electrical, Computer, and Biomedical Engineering, University of Rhode Island, RI, USA. His research focus is on understanding the materials and systems capable of monitoring fine-grain motor movements remotely.

Rassoul Diouf received his B.Sc. degree in Electrical Engineering from the University of Rhode Island, RI, USA, in 2017. He is currently working toward the M.Sc. degree with the Department of Electrical, Computer, and Biomedical Engineering, University of Rhode Island. His research interests include Digital Signal Processing and Biomedical Analytics.

Yalda Shahriari received her B.Sc. in Electrical Engineering from Ferdowsi University, Iran, M.Sc. in Biomedical Engineering from Iran University of Science and Technology, and Ph.D. in Biomedical Engineering from the Old Dominion University of Virginia. She accomplished her postdoctoral studies at University of California, San Francisco (UCSF).
She is currently an Assistant Professor of Biomedical Engineering and the Director of NeuralPC Lab in the Department of Electrical, Computer, and Biomedical Engineering, University of Rhode Island, RI, USA. Her research interests are biomedical signal processing, brain-computer interface (BCI) for assistive technology, statistical analysis and modeling, machine learning algorithms, healthcare units and biomedical data analysis.

Kunal Mankodiya (S'08-M'14) received his B.E. degree in Biomedical Engineering from the Saurashtra University, India, in 2003, M.S. degree in Biomedical Engineering, and the Ph.D. degree in Computer Science from the University of Luebek, Germany in 2007 and 2010, respectively. From 2011 to 2014, he was a postdoctoral researcher at Intel Science and Technology Center (ISTC) affiliated with Carnegie Mellon University (CMU), Pittsburgh, PA, USA.
He is currently an Associate Professor of Biomedical Engineering and the Director of Wearable Biosensing Lab in the Department of Electrical, Computer, and Biomedical Engineering, University of Rhode Island, RI, USA. He enjoys his research on wearable systems, smart textiles, Internet-of-Things, and neural engineering.